

Momentum-constrained Hybrid Heuristic Trajectory Optimization Framework with Residual-enhanced DRL for Visually Impaired Scenarios[★]

Yuting Zeng^a, Zhiwen Zheng^a, You Zhou^a, JiaLing Xiao^b, Yongbin Yu^{*,a}, Manping Fan^{*,a}, Bo Gong^{b,c} and Liyong Ren^a

^aSchool of Information and Software Engineering, University of Electronic Science and Technology of China, Chengdu 610054, Sichuan, P.R. China

^bSichuan Provincial Key Laboratory for Human Disease Gene Study, Sichuan Academy of Medical Sciences & Sichuan Provincial People's Hospital, University of Electronic Science and Technology of China, Chengdu, Sichuan, China.

^cResearch Unit for Blindness Prevention, Chinese Academy of Medical Sciences, Sichuan Academy of Medical Sciences and Sichuan Provincial People's Hospital, Chengdu, Sichuan, China.

ARTICLE INFO

Keywords:

Momentum-constrained residual-enhanced network heuristic trajectory optimization deep reinforcement learning visually impaired scenarios

ABSTRACT

This paper proposes a momentum-constrained hybrid heuristic trajectory optimization framework (MHHTOF) tailored for assistive navigation in visually impaired scenarios, integrating trajectory sampling generation, optimization and evaluation with residual-enhanced deep reinforcement learning (DRL). In the first stage, heuristic trajectory sampling cluster (HTSC) is generated in the Frenet coordinate system using third-order interpolation with fifth-order polynomials and momentum-constrained trajectory optimization (MTO) constraints to ensure smoothness and feasibility. After first stage cost evaluation, the second stage leverages a residual-enhanced actor-critic network with LSTM-based temporal feature modeling to adaptively refine trajectory selection in the Cartesian coordinate system. A dual-stage cost modeling mechanism (DCMM) with weight transfer aligns semantic priorities across stages, supporting human-centered optimization. Experimental results demonstrate that the proposed LSTM-ResB-PPO achieves significantly faster convergence, attaining stable policy performance in approximately half the training iterations required by the PPO baseline, while simultaneously enhancing both reward outcomes and training stability. Compared to baseline method, the selected model reduces average cost and cost variance by 30.3% and 53.3%, and lowers ego and obstacle risks by over 77%. These findings validate the framework's effectiveness in enhancing robustness, safety, and real-time feasibility in complex assistive planning tasks.

1. Introduction

Visually impaired individuals face significant challenges in navigating complex environments due to their limited access to visual cues, such as obstacles, road boundaries, and dynamic agents [1]. In both indoor and outdoor settings, the absence of reliable visual feedback not only increases the risk of collisions and disorientation but also imposes a high cognitive burden when interpreting spatial layouts through auditory [2] or tactile feedback. Here, cognitive burden refers to the mental effort required to process, integrate, and act upon incomplete or indirect environmental information. While conventional assistive tools such as guide dogs [3] offer basic support, they often fall short in dynamic or unfamiliar environments, lacking the ability to proactively sense, interpret, and adapt to changing scenes.

^{*}This work was supported in part by the National Natural Science Foundation of China under Grants 62276055 and 62406062, in part by the Sichuan Science and Technology Program under Grant 2023YFG0288, in part by the Natural Science Foundation of Sichuan Province under Grant 2024NSFSC1476, in part by the National Science and Technology Major Project under Grant 2022ZD0116100, in part by the Sichuan Provincial Major Science and Technology Project under Grant 2024ZDZX0012.

[★]Corresponding authors

✉ 1030839769zengyuting@gmail.com (Y. Zeng); z.z.w@icloud.com (Z. Zheng); 1244568901@qq.com (Y. Zhou); jollyxiao1998@163.com (J. Xiao); ybyu@uestc.edu.cn (Y. Yu^{*}); fmpfmp@uestc.edu.cn (M. Fan^{*}); gongbo@med.uestc.edu.cn (B. Gong); lyren@uestc.edu.cn (L. Ren)

ORCID(s):

These limitations highlight the need for intelligent navigation systems capable of providing safe, smooth, and context-aware motion guidance in real time [4]. Here, context-aware denotes the system's ability to perceive and adapt to dynamic environmental semantics, user intent, and localized spatial structures. The term semantic refers to high-level contextual features such as road topology, trajectory intent, and spatial affordances, which guide decision-making processes beyond purely geometric or kinematic considerations.

Trajectory planning for visually impaired individuals involves challenges beyond general autonomous navigation, requiring agents to operate under sensory limitations [5] while ensuring interpretability and user comfort. This calls for planning frameworks that are not only robust and semantically coherent, but also aligned with human perception and behavior [6]. Here, perceptual refers to sensory-accessible channels such as haptic, auditory, or inferred spatial signals that compensate for limited visual input. To address both physical feasibility and cognitive strain, we adopt a perceptual-aligned, momentum-constrained heuristic strategy that encodes these human sensory limitations into safe, interpretable, and cognitively coherent motion representations.

Existing trajectory optimization methods in robotics typically aim to minimize handcrafted cost functions under

motion constraints. Meta-reviews [7, 8] have further highlighted the deficiencies of existing assistive planning systems, including inadequate environmental modeling, insufficient support for multi-objective balancing [9], and limited adaptability to diverse user preferences and cognitive traits. While some physical interaction frameworks [10] show promise for real-world deployment, their reliance on hardware restricts scalability and excludes algorithmic trajectory optimization. While effective in structured environments, these approaches often fall short when facing real-time, user-centric planning problems.

To address computational and coverage issues, heuristic sampling methods, particularly those that leverage polynomial parameterizations and Frenet-frame abstractions, have been widely employed. The methods [11] allow rapid generation of candidate trajectories and can efficiently explore the planning space. Nonetheless, they typically lack trajectory-level refinement capabilities and fail to incorporate context-aware or social constraints. This becomes especially problematic in human-shared spaces where a trajectory's acceptability depends not just on geometry, but on how well it aligns with human comfort and situational awareness. Heuristic planners also suffer from local suboptimality, particularly when momentum constraints or nonholonomic dynamics are involved. Recent work has also applied DRL in the Frenet frame for lane-change planning with grid-map inputs [12]. However, such methods often lack multi-objective coordination and semantic interpretability, which limits their applicability to assistive and human-centered navigation tasks. These are the issues that our framework aims to address.

Recent advancements in deep reinforcement learning (DRL) have shown promising potential in autonomous navigation tasks, particularly for continuous control and dynamic environments. Comparative evaluations, such as Zhang et al. [13], demonstrate that DDPG outperforms PPO in terms of convergence speed and reward accumulation in driving tasks, although lacking user-specific safety modeling. Other efforts introduce modified PPO variants, such as Beta-distribution-based policies with distributed sampling for ship navigation [14], achieving smoother trajectories and improved robustness, yet still omitting trajectory priors and semantic constraints. These limitations hinder their applicability to assistive scenarios, where human-aligned, interpretable, and context-aware decision-making is critical. In response, our framework integrates heuristic trajectory sampling with residual-enhanced DRL, enabling personalized, safe, and semantically consistent planning tailored for visually impaired users.

To further address the challenges of training stability and temporal coherence in assistive navigation, research incorporates residual blocks and recurrent modeling into the policy architecture. Inspired by works such as ResRace [15] and RSAC [16], we employ residual learning to refine policy outputs by leveraging prior-guided baselines, thereby accelerating convergence and reducing data inefficiency. In parallel, temporal dependencies are modeled through LSTM

modules, as shown effective in dynamic maritime and mobile robot tasks [17, 18], allowing robust sequential decision-making. This residual-temporal structure enhances feature propagation, stabilizes policy updates, and captures task-relevant temporal patterns, significantly improving trajectory consistency and adaptability under noisy, constrained sensory conditions.

Recognizing the limitations of both standalone heuristic and learning-based approaches, hybrid frameworks have emerged to combine the structured guarantees of sampling with the adaptive capacity of DRL. Recent studies have proposed integrating DRL with trajectory sampling[19] or traditional planning pipelines[20] to enhance robustness and adaptiveness. While initial work has shown that such combinations can improve overall trajectory optimization performance, many existing efforts suffer from loose coupling: heuristic methods generate trajectories that are merely used as environment rollouts for DRL, or DRL policies are fine-tuned without feedback to the sampling module. Furthermore, most approaches overlook the importance of multi-objective trajectory evaluation, which involves balancing feasibility, safety, smoothness, and human-centeredness, and is essential for assistive navigation systems.

To address the above limitations, we propose a MHHTOF tailored for visually impaired navigation. The framework integrates structured global HTSCMOE integrating with a residual-enhanced DRL policy, achieving a tight coupling between deterministic efficiency and adaptive robustness. The main contributions of this paper are summarized as follows:

- 1) This work designs a MHHTOF that unifies heuristic sampling with residual-enhanced DRL. A shared multi-objective cost function governs both trajectory generation and policy optimization, achieving coherent and goal-aligned learning across stages.
- 2) To ensure trajectory feasibility and human comfort in assistive scenarios, a dynamic-aware sampling strategy is constructed using third-order interpolation and momentum continuity constraints. This approach effectively generates smooth and kinematically consistent path candidates suitable for real-world execution.
- 3) The study further devises a residual-enhanced actor-critic architecture equipped with LSTM-based temporal modeling, which improves policy representation capability, stabilizes training dynamics, and facilitates adaptive refinement of candidate trajectories under sequential decision-making tasks.
- 4) The novel human-centered DCMM with weight transfer is proposed, where heuristic sampling in the Frenet frame ensures feasibility and comfort via a multi-objective cost function, and reward-driven refinement in the Cartesian frame enhances trajectory quality. A weight transfer mechanism aligns both stages, enabling interpretable and personalized optimization for visually impaired users.

This paper is organized as follows: Section 2 introduces the theoretical foundation and modeling assumptions; Section 3 describes the overall system architecture, including

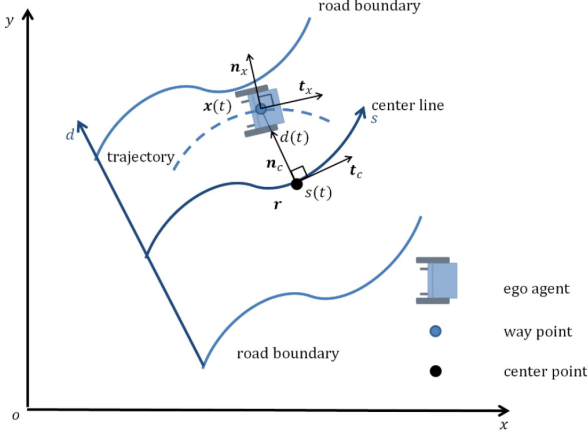


Figure 1. Schematic Diagram of the Conversion Trajectory from the Frenet Coordinate System to the Cartan Coordinate System.

the heuristic sampling and DRL modules; Section 4 presents experimental evaluations and ablation studies; and Section 5 concludes the paper and discusses future work directions.

2. Problem Formulation of Trajectory Optimization for Visually Impaired Scenarios

To support cognitively aligned navigation for visually impaired users, this work adopts a trajectory optimization framework based on the Frenet coordinate system. Drawing inspiration from the way human navigators, especially individuals with visual impairments, align their motion with physical boundaries such as curbs and sidewalk edges, the Frenet-based formulation facilitates a geometry-consistent representation by decoupling longitudinal and lateral motion. This structure facilitates efficient optimization while reflecting perceptual dependencies common in visually guided or tactile-aided mobility [21, 22].

2.1. Coordinate Decoupling for Perceptual-Aligned Motion Representation

The Frenet frame defines local motion along a reference path[23] by projecting the agent's position onto longitudinal and lateral directions. This allows trajectory generation directly over environment-conforming geometries such as sidewalks or pedestrian lanes [24]. Compared with Cartesian coordinates, the Frenet formulation offers superior alignment with how visually impaired individuals perceive motion, as it relies more on edge-following and structured cues rather than global localization [25].

As illustrated in Figure 1, the agent's spatial state is represented by its arc length $s(t)$ and lateral deviation $d(t)$ from a known reference path:

$$\mathbf{x}(s(t), d(t)) = \mathbf{r}(s(t)) + d(t)\mathbf{n}_c(s(t))$$

$$\left\{ \begin{array}{l} s = s(t) \\ d = d(t) \end{array} \right. \quad (1)$$

where $\mathbf{r}(s)$ denotes the position along the reference line, and $\mathbf{n}_c(s)$ is the corresponding normal vector. This representation

introduces natural constraints aligned with sidewalk or path structures, supporting safe, semantically and perceptually meaningful navigation [26]. The full state in the Frenet frame is described as $[s, \dot{s}, \ddot{s}; d, \dot{d}, \ddot{d}, d', d'']$. Here, \dot{s} , \ddot{s} represent longitudinal velocity and acceleration, while d' , d'' reflect lateral variation and curvature smoothness. Such decoupling is well-suited to hierarchical planning and reflects how movement planning by visually impaired individuals is often segmented between directional advancement and lateral path adherence. To support physical realization and control, the Frenet state can be transformed back into Cartesian coordinates through:

$$\mathbf{x}(t) = \mathbf{Q}(x(t), y(t)) = \mathbf{F}(s, d) \quad (2)$$

where

$$\left\{ \begin{array}{l} x_x(t) = \mathbf{F}_x(s(t), d(t)) \\ y_x(t) = \mathbf{F}_y(s(t), d(t)) \end{array} \right. \quad (3)$$

These transformations guarantee geometric consistency and serve as the basis for dynamic feasibility and constraint enforcement in planning. A complete description of the transformation parameters is presented in Table 1[27].

2.2. DCMM Cost Function Design for Human-Centric Planning

To satisfy assistive navigation demands, including smooth maneuvering, proximity buffer, and speed safety, a decoupled multi-objective cost function is first formulated in the Frenet frame for trajectory generation.

$$J[d, s] = J_d[d] + k_s J_s[s], k_s > 0 \quad (4)$$

where $J_d[d]$ penalizes lateral irregularity, such as abrupt curvature changes or deviation from navigable boundaries, and $J_s[s]$ evaluates longitudinal consistency, emphasizing velocity smoothness and deceleration feasibility [28]. This decoupled formulation allows interpretable control over human-centric planning priorities, such as comfort and reactivity to environmental constraints.

Let $\mathcal{T} = \{x^{(1)}(t), x^{(2)}(t), \dots, x^{(N)}(t)\}$ denote the candidate trajectories generated by minimizing $J[d, s]$ and projected to Cartesian space. To incorporate context-aware and dynamic preferences in trajectory selection, a second-stage evaluation is conducted using a DRL-guided adaptive cost function:

$$J_{\text{eval}}^{\text{DRL}}(x^{(i)}(t)) = \sum_{j=1}^n \lambda_j^{\text{DRL}} \cdot \phi_j(x^{(i)}(t)), \quad x^{(i)}(t) \in \mathcal{T} \quad (5)$$

where $\phi_j(\cdot)$ represents interpretable evaluation metrics in the Cartesian space, such as curvature continuity, obstacle clearance, and social compliance, and λ_j^{DRL} denotes adaptive weights learned by the DRL policy network based on current environmental observations.

The final trajectory is selected as:

$$x^*(t) = \arg \min_{x^{(i)}(t) \in \mathcal{T}} J_{\text{eval}}^{\text{DRL}}(x^{(i)}(t)) \quad (6)$$

Table 1

Transformation Parameters from Cartesian to Frenet Coordinates

Symbol	Name	Physical Meaning / Unit	Coordinate System
s	Frenet longitudinal coordinate	Arc length along reference line / m	Frenet
\dot{s}	Frenet longitudinal velocity	Velocity along reference line / m/s	Frenet
\ddot{s}	Frenet longitudinal acceleration	Change rate of longitudinal velocity / m/s ²	Frenet
d	Frenet lateral coordinate	Offset from reference line / m	Frenet
\dot{d}	Frenet lateral velocity	Velocity perpendicular to reference line / m/s	Frenet
\ddot{d}	Frenet lateral acceleration	Change rate of lateral velocity / m/s ²	Frenet
l'	First derivative of lateral offset	Derivative of lateral offset w.r.t. to longitudinal position / -	Frenet
l'''	Second derivative of lateral offset	Change rate of lateral offset w.r.t. to lateral velocity / 1/m	Frenet
x	Cartesian coordinate	Cartesian coordinate system vehicle position (x,y) / m	Cartesian
θ_x	Heading angle	Angle between vehicle heading and x-axis / rad	Cartesian
k_x	Curvature	Curvature of trajectory / 1/m	Cartesian
v_x	Cartesian velocity	Vehicle speed magnitude / m/s	Cartesian
a_x	Cartesian acceleration	Change rate of vehicle speed / m/s ²	Cartesian

Remark 1. Prior approaches[29, 28, 30] that rely solely on Frenet-frame optimization provide efficient sampling and kinematic feasibility but often lack global semantic awareness and adaptability to social contexts. In contrast, methods based only on Cartesian-space learning [31] capture semantic and contextual cues but struggle with geometric consistency and stable motion generation. The proposed dual-stage DCMM framework bridges these limitations by combining curvature-aware sampling in the Frenet frame with DRL-guided evaluation in the Cartesian frame, enabling both interpretable structure and human-aligned adaptability for assistive navigation.

3. MHHTOF with Residual-enhanced DRL

To address the complex needs of assistive navigation for the visually impaired, this study introduces a MHHTOF combining heuristic sampling and residual-enhanced DRL. A Frenet-based front-end generates smoothed trajectories, while a DRL-based back-end adaptively refines them via a residual actor-critic network[32]. A DCMM guides both sampling and learning, with weight transfer ensuring semantic alignment. The framework achieves robust, interpretable, and user-aware path optimization in dynamic settings. The following Figure 2 illustrates the overall architecture of the proposed hybrid optimization framework.

3.1. Design of HTSCMOE for Assistive Navigation

To meet the safety, feasibility, and comfort demands of visually impaired navigation, this section introduces a heuristic front-end for trajectory generation and optimization. Trajectory cluster is sampled in the Frenet frame by varying endpoint states and fitting quintic polynomials, followed by third-order smoothing to ensure temporal continuity. A MTO module enhances physical plausibility and user comfort. The rest trajectories undergo kinematic checks, collision checks, and multi-objective evaluation in Cartesian space. After the dual-stage evaluation, the stage yielding a compact, interpretable input set for downstream DRL-based policy learning. Figure 3 illustrates the overall workflow of HTSCMOE for assistive navigation.

3.1.1. HTSC Generation with Endpoint Smoothing for Visually Impaired Navigation

To meet the real-time, safe, and smooth planning needs of visually impaired navigation, we design a heuristic sampling-based trajectory generation framework. This module constructs a trajectory cluster composed of dynamically feasible, spatially coherent motion candidates that serve as reliable inputs for subsequent cost-aware policy refinement.

1) **HTSC Generation.** Each local trajectory segment within the heuristic sampling process is represented by fifth-order polynomials[33] in the Frenet coordinate system. The longitudinal and lateral motions are decoupled and parameterized respectively as:

$$\begin{cases} s(t) = \sum_{i=0}^5 a_i \times t^i \\ d(s) = \sum_{i=0}^5 b_i \times s^i \end{cases} \quad (7)$$

which

$$\begin{cases} a = [a_0, a_1, a_2, a_3, a_4, a_5] \\ b = [b_0, b_1, b_2, b_3, b_4, b_5] \end{cases} \quad (8)$$

Here, $s(t)$ denotes longitudinal evolution over time, while $d(s)$ captures lateral deviation with respect to the longitudinal displacement. This representation maintains coupling expressivity while enabling efficient computation. Given the boundary state (position, velocity, acceleration) at both the start and end of each segment, the coefficients a_i and b_i are computed analytically:

For longitudinal motion:

$$\begin{aligned} a_{[0:2]} &= [s(t_0), \dot{s}(t_0), \frac{1}{2}\ddot{s}(t_0)] \\ a_{[3:5]} &= \text{Solve } (\mathbf{A}_1, \mathbf{B}_1) \end{aligned} \quad (9)$$

For lateral motion:

$$\begin{aligned} b_{[0:2]} &= [d(t_\tau), \dot{d}(t_\tau), \frac{1}{2}\ddot{d}(t_\tau)] \\ b_{[3:5]} &= \text{Solve } (\mathbf{A}_2, \mathbf{B}_2) \end{aligned} \quad (10)$$

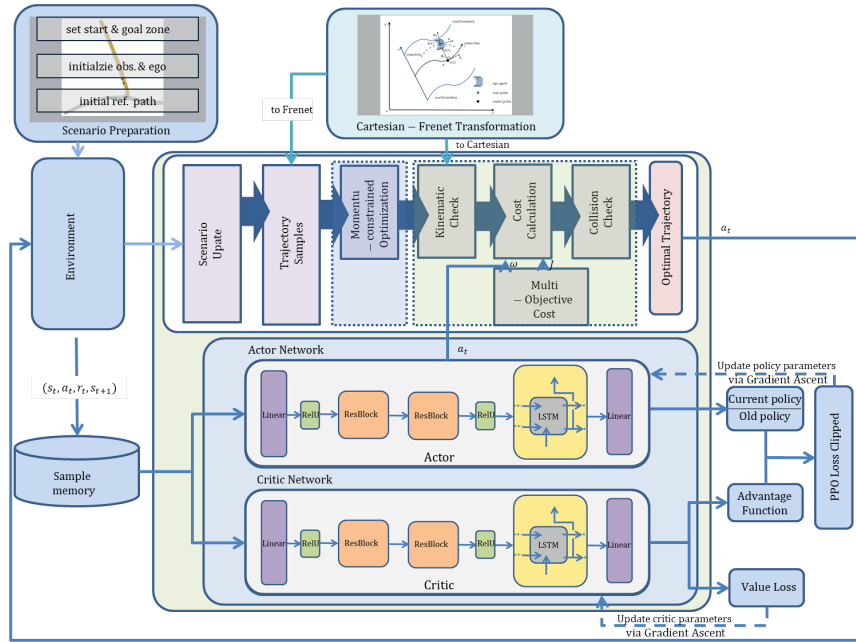


Figure 2. Overall Architecture of the Proposed Hybrid Optimization Framework.

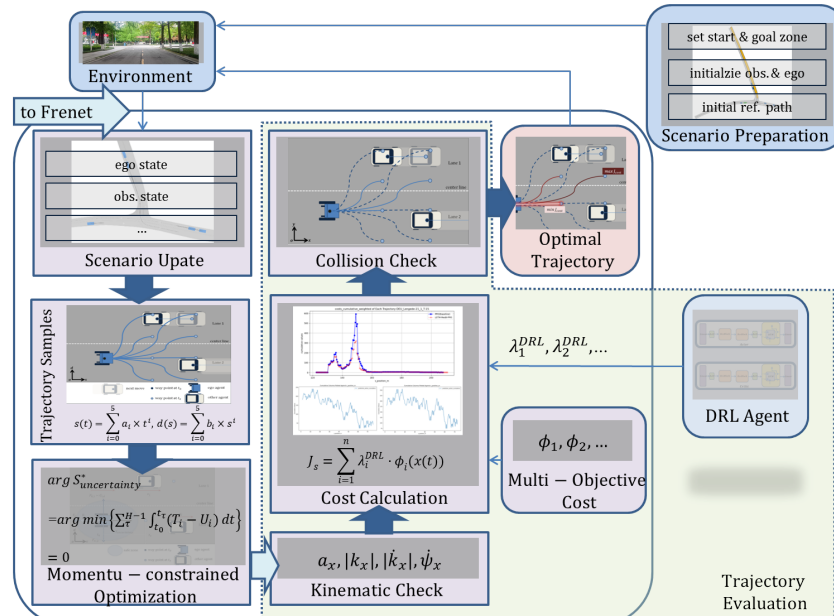


Figure 3. Flowchart of HTSCMOE for Assistive Navigation.

$$\mathbf{A}_1 = \begin{bmatrix} (t_\tau - t_0)^3 & (t_\tau - t_0)^4 & (t_\tau - t_0)^5 \\ 3 \times (t_\tau - t_0)^2 & 4 \times (t_\tau - t_0)^3 & 5 \times (t_\tau - t_0)^4 \\ 6 \times (t_\tau - t_0) & 12 \times (t_\tau - t_0)^2 & 20 \times (t_\tau - t_0)^3 \\ s(t_\tau) - a_0 - a_1 \cdot (t_\tau - t_0) - a_2 \cdot (t_\tau - t_0)^2 \\ \dot{s}(t_\tau) - a_1 - 2 \times a_2 \cdot (t_\tau - t_0) \\ \ddot{s}(t_\tau) - 2 \times a_2 \end{bmatrix} \quad (11)$$

$$\mathbf{A}_2 = \begin{bmatrix} S_{\tau_0}^3 & S_{\tau_0}^4 & S_{\tau_0}^5 \\ 3 \times S_{\tau_0}^2 & 4 \times S_{\tau_0}^3 & 5 \times S_{\tau_0}^4 \\ 6 \times S_{\tau_0} & 12 \times S_{\tau_0}^2 & 20 \times S_{\tau_0}^3 \\ d(t_\tau) - b_0 - b_1 \cdot S_{\tau_0} - b_2 \cdot S_{\tau_0}^2 \\ \dot{d}(t_\tau) - b_1 - 2 \times b_2 \cdot S_{\tau_0} \\ \ddot{d}(t_\tau) - 2 \times b_2 \end{bmatrix} \quad (12)$$

Here, \mathbf{A}_1 , \mathbf{B}_1 and \mathbf{A}_2 , \mathbf{B}_2 are time-dependent coefficient matrices derived from endpoint constraints[34] and S_{τ_0} equals $s(t_\tau) - s(t_0)$. This formulation guarantees that each sampled

trajectory within the cluster adheres to dynamic feasibility and maintains smoothness at the terminal points, satisfying physical constraints crucial for user stability in assistive guidance.

2) **Endpoint Smoothing via Third-Order State Interpolation.** To enhance the temporal continuity across the sampled trajectory cluster, we apply a terminal-state-aware smoothing model that explicitly aligns position, velocity, and acceleration across segments. For any dimension $\xi_i(t) \in \{s(t), d(t)\}$, the dynamic state is interpolated as:

$$\begin{cases} \xi_{i_1}(t) = \sum_{j=0}^5 c_j t^j, \\ \xi_{i_2}(t) = \dot{\xi}_{i_1}(t) = \sum_{j=1}^5 j c_j t^{j-1}, \\ \xi_{i_3}(t) = \ddot{\xi}_{i_1}(t) = \sum_{j=2}^5 j(j-1) c_j t^{j-2} \end{cases} \quad (13)$$

Given the endpoint states $\xi_i(0) = [\xi_{i_1}(0), \xi_{i_2}(0), \xi_{i_3}(0)]^\top$ and $\xi_i(\tau) = [\xi_{i_1}(\tau), \xi_{i_2}(\tau), \xi_{i_3}(\tau)]^\top$, the coefficients c_i are solved analytically to ensure smooth junction transitions within the trajectory cluster. This is especially critical in human-centered planning where abrupt changes may compromise comfort or cause disorientation for visually impaired users.

The proposed heuristic sampling module generates a structured trajectory cluster that integrates polynomial-based modeling and endpoint-aware smoothing. This design enhances spatial and temporal continuity, enabling robust downstream decision-making. By embedding feasibility, comfort, and adaptability into the initial trajectory set, this module lays a reliable foundation for assistive navigation tailored to the unique needs of the visually impaired.

3.1.2. MTO for Visually Impaired Scenarios

Building upon the system modeling and problem formulation presented in Section 2.1.1, this study further investigates trajectory optimization in dynamic environments, specifically targeting assistive needs for visually impaired individuals. $\xi(t)$ is the value of the state variable.

$$\xi(t) = [s(t), \dot{s}(t), \ddot{s}(t), d(t), \dot{d}(t), \ddot{d}(t)] \quad (14)$$

The continuous time state space model of the system and the linear observation structure of the output function can be expressed as[35]:

$$\begin{aligned} \dot{\xi}(t) &= \begin{bmatrix} A & \mathbf{0} \\ \mathbf{0} & A \end{bmatrix} \xi(t) + \begin{bmatrix} B & \mathbf{0} \\ \mathbf{0} & B \end{bmatrix} u(t) \\ y(t) &= \begin{bmatrix} C & \mathbf{0} \\ \mathbf{0} & C \end{bmatrix} \xi(t) + \begin{bmatrix} D & \mathbf{0} \\ \mathbf{0} & D \end{bmatrix} u(t) \in \mathcal{R}(t) \\ &= E\xi(t) \end{aligned} \quad (15)$$

where

$$A = \begin{bmatrix} 0 & 1 & 0 \\ 0 & 0 & 1 \\ 0 & 0 & 0 \end{bmatrix}, B = \begin{bmatrix} 0 \\ 0 \\ 1 \end{bmatrix} \quad (16)$$

The trajectory optimization objective for each agent is to achieve an optimal trade-off between safety and efficiency.

This trajectory optimization problem is formalized accordingly:

$$S = \lim_{N \rightarrow \infty} \frac{1}{N} \sum_{k=0}^{N-1} J(u(t_k), \xi(t_k), \Phi) \quad (17)$$

To address this, a trajectory cost modeling framework is proposed based on the Lagrangian function L_i , incorporating a dynamic evaluation function $S_{\text{uncertainty}}$ to assess the system's ability to sustain state stability and regulate uncertainty within a specified temporal horizon:

$$S_{\text{uncertainty}} = (t_\tau - t_0) \cdot \mathbb{E}_{t \in [t_0, t_\tau]} [L_i(t)] \quad (18)$$

, where

$$L_i(t) = E_{\text{motion},i}(t) - E_{\text{guidance},i}(t) \quad (19)$$

In this formulation, $E_{\text{motion},i}$ represents the agent's kinetic energy, while $E_{\text{guidance},i}$ reflects potential energy induced by environmental constraints such as road signs, speed limits, and the behaviors of surrounding agents in assistive navigation scenarios. By modeling the agent's longitudinal and lateral control behavior, an optimal control objective is established:

$$\begin{aligned} u^* = \arg \min_{u_{0:H}} & \left[\int_{t_0}^{t_0 + H\Delta t} L_i(u(t), \xi(t), \Phi) dt \right. \\ & \left. + Z(\xi(t_0 + H\Delta t), \Phi) \right] \end{aligned} \quad (20)$$

To accommodate the dynamic interaction features of complex traffic environments, the system is modeled as a collection of binary agent-interaction systems. In practical mobility scenarios involving visually impaired pedestrians, the interactions are primarily characterized by car-following and lane-changing behaviors, each exhibiting directional asymmetry. Accordingly, a constrained Lagrangian model is constructed that incorporates longitudinal speed limits and lateral road boundaries. A schematic of the momentum-aware trajectory optimization process based on this model is shown in Figure 4.

$$\begin{aligned} L_i(t) = & E_{\text{motion},i}(t) - E_{\text{guidance},i}(t) \\ = & \underbrace{\frac{1}{2} m_i \|v_i(t)\|^2}_{\text{locomotion energy}} - \underbrace{F_{\text{guidance}}(t) \cdot v_i(t)}_{\text{haptic/audio interaction}} \\ & - \underbrace{F_{\text{crowd}}(t) \cdot (v_i(t) - v_j(t))}_{\text{social compliance}} + \underbrace{\lambda_s \|\dot{v}_i(t)\|^2}_{\text{smoothness regularization}} \\ & + \underbrace{\lambda_u \cdot \text{Tr} \left[\Sigma_i^{\text{perception}}(t) \right]}_{\text{perceptual uncertainty penalty}} \end{aligned} \quad (21)$$

In Eq. 21, m_i is the mass of vehicle i , and $v_i(t)$ and $v_j(t)$ denote the velocities of agent i and its neighboring agent j ,

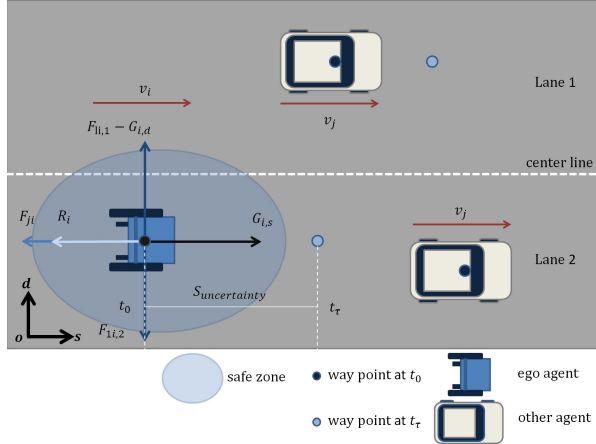


Figure 4. Schematic of MTO Process for Visually Impaired Scenarios.

respectively. $\mathbf{F}_{\text{guidance}}(t)$ and $\mathbf{F}_{\text{crowd}}(t)$ represent external forces arising from guidance systems and social interactions.

The last two terms model regularization effects: λ_s penalizes abrupt accelerations to ensure smoothness, while λ_u regulates perceptual uncertainty via the trace of the perception covariance matrix $\Sigma_i^{\text{perception}}(t)$.

To incorporate social navigation constraints reflective of limited perception in visually impaired scenarios, we adopt an anisotropic interaction model inspired by perceptual field theory [36, 37]. The resulting repulsive force from surrounding agents is expressed as:

$$\mathbf{F}_{\text{crowd}}^{i,j}(t) = \frac{1}{2} m_j \left\| \mathbf{v}_j(t) \right\|^2 \cdot \mathbf{r}_{ij}(t) \left(\frac{1}{r_s^2(t)} - \frac{1}{r_d^2(t)} \right) \cdot \mathbf{n}_{ij}(t) \quad (22)$$

Here, the formulation captures directionally modulated collision avoidance behavior, where $r_s(t) = r_{ij,s}(t) + B_{\text{safe},s}$ and $r_d(t) = r_{ij,d}(t) + B_{\text{safe},d}$ represent longitudinal and lateral safety thresholds within an elliptical perceptual domain. This structure emphasizes the user's forward-focused awareness and risk asymmetry, enabling the planner to prioritize deceleration or avoidance in a way that aligns with real-world visual compensation strategies.

Furthermore, the assistive driving intention is modeled by mapping user mobility goals into a driving force formulation that considers road slope perception and traffic regulations, incorporating vehicle mass, gravitational acceleration, and velocity intention to better align with the control needs of visually impaired users.

The guidance-related interaction term $\mathbf{F}_{\text{guidance}}(t) \cdot \mathbf{v}_i(t)$ comprises two components: the longitudinal guidance force $G_{i,s}(t)$ derived from slope-aware system commands, and the lateral lane-constraining force $F_{\text{li}}(t)$ that models tactile or auditory lane boundary feedback[29].

$$\mathbf{F}_{\text{guidance}}(t) = \underbrace{m_i g \sin \varphi_{i,s}(t)}_{\text{longitudinal guidance}} \cdot \mathbf{e}_s + \underbrace{m_i B_{\text{type}} \left(\frac{w}{2} - r_{\text{li}}(t) \right)}_{\text{lateral lane feedback}} \cdot \mathbf{e}_d$$

(23)

Specifically,

$$\mathbf{F}_{\text{guidance}}(t) = \begin{bmatrix} F_{\text{guidance},s}(t) \\ F_{\text{guidance},d}(t) \end{bmatrix} = \begin{bmatrix} -G_{i,s}(t) \\ F_{\text{li}}(t) - G_{i,d}(t) \end{bmatrix} \quad (24)$$

where $\sin \varphi_{i,s}(t) = \lambda B_{\text{bump}} \frac{v_{\text{desire}}(t)}{v_{\text{law}}(t)}$, with $v_{\text{desire}}(t)$ and $v_{\text{law}}(t)$ denoting the desired velocity and the prescribed velocity, respectively, while B_{bump} can mitigate the impact of bumps. B_{type} denotes the line shape of the road boundary, and the value of this parameter is fixed due to dataset characteristics[38, 39]. n_{li} is the distance between the vehicle and the road boundary, and w is the lane width. The unit vectors \mathbf{e}_s and \mathbf{e}_d represent the longitudinal and lateral axes in the local motion frame.

Finally, the Lagrangian functions of longitudinal L_s and lateral L_d motion are decomposed and optimized within the Frenet coordinate framework through a backtracking approach, resulting in a spatiotemporally coupled trajectory planner.

$$\left\{ \begin{array}{l} L_s = \int_{t_0}^{t_\tau} \left[\frac{1}{2} m_i \dot{v}_{i,s}^2(t) - (G_{i,s}(t) + F_{\text{crowd},s}(t)) v_{i,s}(t) \right. \\ \quad \left. + \lambda_s \dot{v}_{i,s}^2(t) + \lambda_u \cdot \text{Tr} \left[\Sigma_i^{\text{perception}}(t) \right] \right] dt \\ L_d = \int_{t_0}^{t_\tau} \left[\frac{1}{2} m_i \dot{v}_{i,d}^2(t) - (F_{\text{li}}(t) - G_{i,d}(t) + F_{\text{crowd},d}(t)) \right. \\ \quad \left. \cdot v_{i,d}(t) + \lambda_s \dot{v}_{i,d}^2(t) + \lambda_u \cdot \text{Tr} \left[\Sigma_i^{\text{perception}}(t) \right] \right] dt \end{array} \right. \quad (25)$$

The Euler-Lagrange equations are utilized for trajectory solution:

$$\frac{d}{dt} \left(\frac{\partial L}{\partial \dot{\xi}_i} \right) - \left(\frac{\partial L}{\partial \xi_i} \right) + \frac{d^2}{dt^2} \left(\frac{\partial L}{\partial \ddot{\xi}_i} \right) = 0 \quad (26)$$

where the generalized coordinate $\xi_i(t)$ encapsulates both longitudinal and lateral kinematics in the Frenet frame. This formulation enables the trajectory planner to reason jointly about directional feasibility and optimality.

Remark 2. To meet the specific demands of assistive navigation, the proposed Lagrangian framework integrates several human-centered modeling innovations. The guidance interaction term $\mathbf{F}_{\text{guidance}}(t)$ incorporates slope-sensitive modulation through B_{bump} , which mitigates abrupt velocity changes caused by terrain irregularities. This is an essential design for two-wheel assistive devices prone to instability on uneven surfaces. The lateral correction force embeds B_{type} , capturing fixed infrastructure characteristics, thereby enhancing model generalization across varying road geometries. Additionally, the repulsive force $\mathbf{F}_{\text{crowd}}(t)$ adopts a hard-coded informed asymmetric safety buffer, explicitly extending protective zones to account for the reduced environmental awareness of visually impaired users. Finally, the

perceptual uncertainty term $\text{Tr}[\Sigma_i^{\text{perception}}(t)]$, together with tunable weights λ_s and λ_u , reflects the impact of sensor noise and latency, enabling the planner to balance comfort-aware smoothness with robustness to degraded inputs.

3.1.3. Trajectory Evaluation for Visually Impaired Scenarios

In assistive trajectory optimality for visually impaired individuals, each candidate trajectory undergoes a dual-stage inspection process to ensure both physical feasibility and human-centric quality. This mechanism not only eliminates unsafe or unrealizable paths, but also encodes informative gradient feedback for downstream policy refinement.

1) **Feasibility Screening via Kinematic and Collision Checks.** Each optimized trajectory is first screened for feasibility. A kinematic check ensures compliance with motion constraints such as acceleration, yaw rate and curvature limits[40], while a collision check filters out paths that approach obstacles too closely. This step guarantees that only physically valid and safe trajectories proceed to semantic evaluation, serving as a critical safeguard in assistive planning for visually impaired users.

2) Multi-Objective Cost Evaluation in Cartesian Frame.

Trajectories passing the feasibility check are subsequently assessed through a structured, semantically aligned cost function in the Cartesian frame. This stage focuses on qualities that are essential for visually impaired users, including path smoothness, obstacle safety margin, and socially compliant motion.

Each trajectory $x(t)$ is evaluated using a weighted sum of interpretable cost descriptors:

$$J_s = \sum_{i=1}^n \lambda_i^{\text{DRL}} \cdot \phi_i(x(t)) \quad (27)$$

where, $\phi_i(x(t))$ denotes key evaluation metrics, and λ_i^{DRL} represents dynamic weighting coefficients predicted by the policy network based on context-aware features and user preferences. The instantiated terms include Acceleration Energy (AE), Jerk Minimization (JM), Velocity Optimality (VO), Path Deviation (PD), Obstacle Proximity Penalty (OPP), Risk Field Penalty (RFP), and Social Compliance (SC).

$$\left\{ \begin{array}{ll} \phi_1(x) = \int a_x^2(t) dt & (\text{AE}) \\ \phi_2(x) = \int j_x^2(t) dt & (\text{JM}) \\ \phi_3(x) = \int |v_x(t) - v_{\text{desire}}(t)| dt + (v_x(t_f) - v_{\text{desire}}(t_f))^2 & (\text{VO}) \\ \phi_4(x) = \int d^2(t) dt & (\text{PD}) \\ \phi_5(x) = \int \frac{1}{\Delta x_{\text{obs}}^2(t)} dt & (\text{OPP}) \\ \phi_6(x) = \int f(x, 0, \Sigma_{\text{rot}}) dx dt & (\text{RFP}) \\ \phi_7(x) = \int \frac{1-t/T}{d_M(v_j(t), v_x(t), \Sigma(t))} dt & (\text{SC}) \end{array} \right. \quad (28)$$

Remark 3. This cost structure supports two critical roles: it enables semantic ranking among feasible plans, and it provides dense, human-aligned learning signals for downstream DRL-based policy optimization[41]. By replacing

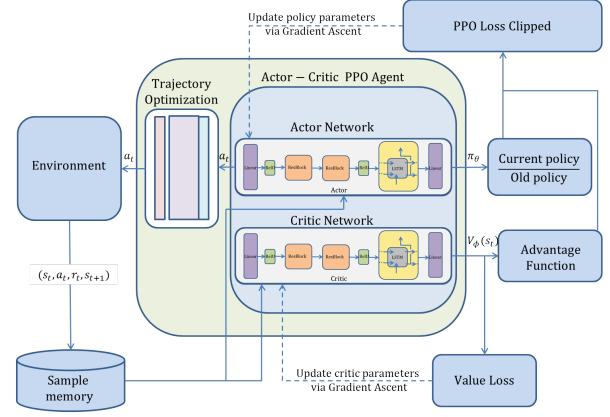


Figure 5. Proposed Residual-enhanced DRL Framework with Temporal Modeling based on PPO.

sparse or binary rewards with interpretable cost gradients, the learning agent gains better generalization ability and convergence stability. This is particularly vital in visually impaired navigation, where avoiding abrupt maneuvers, unsafe detours, or proximity violations is not just preferred but essential for user trust and safety.

3.2. Design of Residual-enhanced DRL Framework for Visually Impaired Scenarios

The proposed Residual-enhanced DRL framework extends the standard Proximal Policy Optimization (PPO) paradigm[42], while introducing residual temporal modeling, heuristic sampling, and structured reward design to address the challenges of assistive navigation. These enhancements improve robustness and adaptability beyond the baseline PPO formulation.

The policy network (actor) selects actions, while the value network (critic) estimates returns; for clarity, "policy" and "actor" are used interchangeably hereafter. Likewise, "reward" reflects the cost-aligned signal guiding learning. As shown in Figure 5, the agent iteratively encodes state, infers actions, and adapts via feedback to ensure robust, user-aligned planning.

3.2.1. Residual-enhanced and Temporal Feature Modeling for Policy and Reward Networks

To address the complex demands of assistive navigation for the visually impaired, where decisions must be robust, temporally stable, and semantically grounded, this work proposes a unified architecture termed ResBlocksCustomPolicyRewardNet. This architecture is applied to both the policy network and the reward network, with independent parameters to ensure functional decoupling. The design enhances expressiveness through residual modeling and captures temporal dependencies via lightweight LSTM modules[43].

The policy and reward networks adopt a unified yet modular architecture, carefully designed to balance expressive capacity and computational efficiency. Both networks follow the same architectural skeleton, wherein the input state

is first projected into a compact intermediate representation. This representation is then processed through multiple stacked residual blocks, which enable deeper feature transformation while preserving gradient flow and supporting shortcut connections even in the presence of dimensional mismatches.

Traditional shallow MLPs often lack sufficient capacity to extract rich semantic and spatial features, especially in safety-critical scenarios such as blind-assistive navigation. To overcome this limitation, each network integrates a stack of Residual Blocks (ResBlocks) [44], which enhance nonlinear expressiveness while preserving gradient flow. Each ResBlock is defined as:

$$\text{ResBlock}(x) = f(x) + S(x) \quad (29)$$

, where

$$S(x) = \begin{cases} x, & \text{if } \dim(x) = \dim(f(x)) \\ W_s x, & \text{otherwise} \end{cases} \quad (30)$$

Here, $f(x)$ denotes a two-layer nonlinear transformation composed of a linear projection followed by a ReLU activation, while $S(x)$ represents the shortcut pathway that ensures identity mapping or a learnable linear projection when dimensional mismatch occurs.

Remark 4. *The policy and value branches in the proposed architecture incorporate lightweight residual blocks tailored for fully connected networks. These blocks utilize identity or linear projections as shortcut connections to ensure dimensional consistency, while maintaining minimal parameter overhead. By avoiding heavy normalization layers and excessive depth, this design retains the benefits of residual learning such as improved gradient flow and stability, while avoiding unnecessary complexity. This facilitates faster convergence and better generalization in policy learning under limited training budgets.*

This flexible design supports consistent multi-layer construction and facilitates deep feature abstraction. The residual-enhanced structure is adopted identically in both the policy and reward networks. Although structurally similar, each network maintains its own independent parameter set. This design ensures that policy learning and reward inference remain functionally isolated, thereby reducing mutual interference and enhancing task-specific generalization.

Beyond static feature modeling, temporal continuity is critical for generating smooth trajectories and learning stable reward dynamics. To this end, a lightweight LSTM is introduced after the residual layers in both networks:

$$h_t = \text{LSTM}(x_t^{\text{Res}}, h_{t-1}, c_{t-1}) \quad (31)$$

where x_t^{Res} is the output from stacked residual layers. This design choice enables the LSTM to operate on high-level encoded features rather than raw inputs, improving efficiency and interpretability.

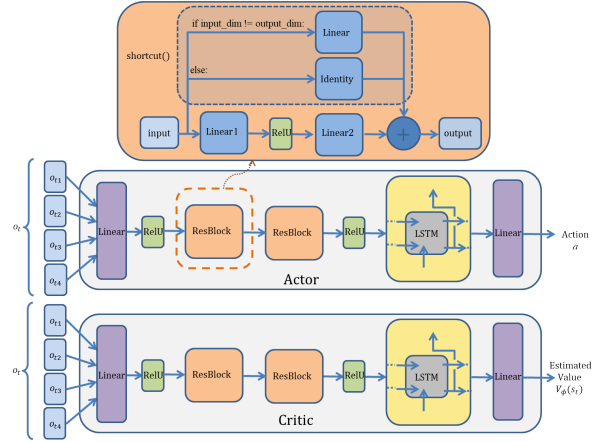


Figure 6. Residual-enhanced Temporal Architecture for Actor Network and Critic Network, Where the Policy and Reward Networks Correspond to the Actor and Critic Components, Respectively.

The LSTM module is designed with controlled dimensionality, such as using eight hidden units, to facilitate deployment on resource-constrained platforms. The final outputs, whether action logits in the policy network or scalar reward estimates in the reward network, are generated through simple linear projection layers.

$$\text{output} = \text{Linear}(h_t) \quad (32)$$

Remark 5. *To capture temporal dependencies in agent-environment interactions without compromising computational efficiency, a compact LSTM module is integrated after the residual-enhanced MLP backbone. With a hidden dimension of only 8, the LSTM effectively models sequential patterns in latent features while preserving low inference latency. This lightweight temporal modeling strategy balances expressiveness and deployment feasibility, making it particularly suitable for real-time assistive navigation tasks where response delay and model size are critical factors.*

Finally, a linear output layer produces either action weights in the policy network or scalar reward estimates in the reward network. While both networks share the same structural design, their parameters are fully independent, ensuring functional decoupling between decision-making and reward modeling. The overall network designs are illustrated in Figure 6, and the architectures are shown in Table 2 and 3.

3.2.2. Context-Aware Policy Modeling for Visually Impaired Scenarios

1) Observation Space with Semantic and Risk Encoding. To accommodate the perceptual limitations of visually impaired users, the observation space is explicitly designed to reflect cognition-based environmental understanding rather than direct visual feedback[45]. The agent's state vector o_t^{cog} integrates dynamic estimates and semantically meaningful spatial cues that can be indirectly inferred

Table 2
Policy Network Architecture

Module	Sub-components	Output Dimensions	Activation Function
Feature Extractor	FlattenExtractor	-	-
Policy MLP	Linear (4→32), ResBlock (×2), ReLU	100	ReLU
Policy Memory Unit	LSTM (100→8)	8	-
Policy Output Head	Linear (8→2)	2	-

Table 3
Reward Network Architecture

Module	Sub-components	Output Dimensions	Activation Function
Feature Extractor	FlattenExtractor	-	-
Value MLP	Linear (4→32), ResBlock (×2), ReLU	100	ReLU
Value Memory Unit	LSTM (100→8)	8	-
Value Output Head	Linear (8→1)	1	-

through auxiliary sensors or environmental feedback. Formally, it is defined as:

$$\begin{aligned} o_t^{\text{cog}} = & \{ \hat{v}_t, \hat{a}_t, \hat{\omega}_t, \theta_t, \\ & d_{\text{goal}}, t_{\text{remain}}, \mathbf{1}_{\text{goal}}, \\ & \phi_{\text{lane}}^L, \phi_{\text{lane}}^R, \rho_{\text{obs}}, \\ & \eta_{\text{valid}}, F_{\text{feas}}, \mu_F, \sigma_F, p_{\text{risk}}^{\text{cog}} \} \end{aligned} \quad (33)$$

where, variables such as \hat{v}_t , ρ_{obs} , and $p_{\text{risk}}^{\text{cog}}$ represent estimated motion states, obstacle proximity, and perceived collision risk, respectively. Features like F_{feas} , μ_F , and σ_F quantify the feasibility and variability of candidate trajectories, thereby emulating how visually impaired users cognitively assess navigability. Semantic lane features $\phi_{\text{lane}}^{L/R}$ substitute direct lane-line detection with probabilistic alignment cues. This structured observation design enables the policy to simulate human-like navigation under constrained perception.

Remark 6. The proposed cognitive observation space o_t^{cog} introduces semantically structured and compact representations. Environmental cues are refined, such as decomposing road context into left and right lane directions, while trajectory-related cost and risk features are integrated into a unified feasibility-aware representation. This design reduces observation dimensionality and enhances learning efficiency, better aligning with the structured, focused perception style of visually impaired users.

2) Action Space via Cost Weight Adaptation. Instead of directly producing low-level motor commands, the reinforcement learning agent modulates trajectory optimization priorities by adjusting the dynamic weights λ_i^{DRL} used in the above semantic cost evaluation. This abstraction introduces a high-level action space aligned with how visually impaired individuals naturally prioritize comfort, safety, and efficiency[46]. The action at time t is formulated as:

$$\lambda_i^t = \text{clip}(\lambda_i^{t-1} + \Delta\lambda_i^{\text{DRL}}, \lambda_i^{\min}, \lambda_i^{\max}) \quad (34)$$

This adaptive mechanism enables the policy to regulate conflicting objectives based on context awareness[47], such

as slowing down near dense obstacles, prioritizing comfort in complex geometries, or accelerating in open and safe regions. The clipped update scheme ensures interpretability and temporal stability, which is particularly critical for the trustworthiness and reliability of assistive navigation systems deployed in real-world environments for visually impaired users.

3) Hierarchical Reward Design for Multi-Level Guidance. To faithfully capture the multifaceted requirements of assistive navigation for visually impaired individuals, we formulate a three-layer hierarchical reward structure that aligns reinforcement signals with real-world cognitive and behavioral objectives. The overall reward at each timestep r_t is computed as:

$$r_t = \sum_{l \in \{ \text{task, behav, risk} \}} \lambda_l \cdot \sum_k r_t^{(l,k)} \quad (35)$$

where λ_l indexes the semantic layer corresponding to task completion *task*, behavioral quality *behav*, and risk sensitivity *risk*, and denotes the configurable layer-wise weight that reflects user-specific preferences or environmental context.

At the task level, rewards reflect successful and timely path completion, penalizing failures such as collisions, timeouts, or infeasible routes. This component models the cognitive emphasis placed by visually impaired users on reaching destinations safely and efficiently. Beyond task success, behavioral feedback is provided based on trajectory smoothness, progress efficiency, and deviation from optimal reference paths. These criteria are closely associated with perceived comfort and system-level interpretability [48]. Finally, a risk-sensitive component penalizes behaviors that indicate potential danger, such as excessive speed or proximity to obstacles, mirroring the heightened safety awareness characteristic of visually impaired navigation. This structured reward mechanism is shown in Table 4.

Remark 7. Unlike traditional reward designs that separate sparse termination rewards and dense behavioral metrics, our hierarchical formulation introduces a semantically

Table 4

Context-Aligned Hierarchical Reward Design for Visually Impaired Navigation

Reward Layer	Objective	Reward Signal	Mathematical Expression	Cognitive Description
Task Guidance Layer	Task completion, path feasibility	Task result feedback Completion timing feedback	r_t^{comp} $r_{\text{goal}}^+, r_{\text{goal}}^-$	Success, timeout, or infeasibility judgment from global cognition Reward early task completion, penalize delay in cognition-based planning
	Driving quality, efficiency, comfort	Reference alignment deviation Speed deviation penalty Goal distance reduction Cost-optimality bias	δ_{align} $\delta_v^{\text{smooth}} = v_t - v_{\text{target}} $ δ_g^{prog} $\Delta C^{\text{cog}} = C_{\text{min}} - C_{\text{ego}}$	Penalize lateral deviation from preferred navigation corridor Encourage speed consistency for smoother user-perceived motion Reward forward progress toward perceived goal direction Encourage selection of cognitively efficient trajectory
Risk Avoidance Layer	Robustness, risk minimization	Self-action risk Environmental risk	$\rho_{\text{self}}^{\text{risk}}$ $\rho_{\text{obs}}^{\text{risk}}$	Penalize over-speeding, unsafe acceleration, or collision probability Penalize proximity to static obstacles or road edges

structured reward mechanism aligned with real-world assistive priorities. By organizing learning signals into task completion, behavioral quality, and risk sensitivity layers, this approach enables interpretable training, flexible customization, and closer alignment with the cognitive, safety, and comfort demands of visually impaired navigation. It thereby fills a critical gap in the integration of goal, behavior, and risk dimensions.

4. Results & analysis

4.1. Environment and training setup

This study leverages the CommonRoad benchmark[49], developed by the Technical University of Munich, as the foundation for training and evaluating assistive navigation agents. Although originally designed for autonomous driving research, CommonRoad provides structured and modular traffic scenarios involving dynamic agents, temporal-spatial constraints, and road topologies. Its open and composable architecture, along with an extensive scenario tagging system, enables strong cross-domain transferability. These characteristics make it a technically robust and adaptable basis for navigation tasks in visually impaired assistance settings.

Although the CommonRoad dataset was not originally designed for human-centered navigation tasks, many of its inherent features, such as structured urban road layouts, signalized intersections, densely populated obstacle regions, and dynamic interactions among surrounding vehicles, exhibit strong similarities to the environmental conditions typically encountered in real-world assistive navigation scenarios. In this work, we maintain the original dataset structure while selectively curating a subset of scenarios that align with human-centered navigation characteristics. The

selection process prioritizes urban semantic tags such as *URBAN* and *INTERSECTION*, a moderate number of dynamic obstacles typically ranging between 3 and 10, lower initial velocities within the range of 2 to 8m/s , and goal specifications that align with assistive navigation tasks, including *LANELET* and *TIME_STEP*. Several of the selected scenarios include representative features, for example left turns, oncoming traffic, and two-lane road segments, which enhance their relevance to real-world assistive contexts and increase their potential for successful knowledge transfer.

By reusing and repurposing these scenarios without modifying the underlying dataset structure, we construct a reproducible yet sufficiently challenging simulation environment tailored to the development of generalizable and interpretable assistive agents for visually impaired users.

The experiment adopts a modular design, standardizes the environment interface through Gymnasium, builds a deep reinforcement learning training environment, ensures the compatibility between the algorithm and the environment, and supports the custom observation space and reward function to meet different research needs.

In terms of algorithm implementation, the algorithm in this study is implemented based on the Stable-Baselines3 library, and the PyTorch deep learning framework is used to construct a customized policy network and value network to enhance the nonlinear expressive ability of the algorithm.

The training process implements stage and summary evaluation monitoring: the experiments record key metrics including episode reward, strategy entropy, and value loss via TensorBoard; intermediate model checkpoints are automatically saved every 40,000 steps; and an early-stop mechanism is set up to terminate the training when there is no significant improvement in 10 consecutive evaluations.

Table 5
Table of Hyperparameters

Hyperparameter	Description	Value
l	Learning rate	0.0003
ϵ	Clipping hyperparameter	0.1
γ	Discount factor	0.80
λ	GAE	0.97
B	Batch size	2352
N^E	Number of training epochs	5
c_2	Entropy coefficient	0.01

The experimental hardware platform is configured as follows:

- Computing unit: 4×NVIDIA GeForce RTX 4090 GPUs (24GB video memory/card)
- System memory: 128GB DDR5
- Storage system: 2TB NVMe SSD

The simulation dataset is divided into training and test sets. To ensure convergence, parallel training is performed with over 10^6 time steps, and the best model is selected after approximately 5×10^5 steps based on reward performance in evaluation scenarios.

Considering the sensitivity of deep reinforcement learning to hyperparameters, key values are determined through repeated tuning. The learning rate is set to $l = 3 \times 10^{-4}$, the PPO clipping parameter to $\epsilon = 0.1$, and the generalized advantage estimation parameter to $\lambda = 0.97$, balancing bias and variance. A discount factor of $\gamma = 0.97$ is used to account for long-term rewards. Each epoch consists of 5 updates with a batch size of 2352, and the entropy coefficient $c_2 = 0.01$ ensures a balance between exploration and exploitation.

These settings ensure algorithmic stability and computational efficiency, forming the basis for subsequent comparative and ablation experiments. The full hyperparameter configuration is listed in Table 5.

4.2. Structural Evaluation: Temporal Modeling and Residual Enhancement

To evaluate the effectiveness of structural enhancements in the proposed trajectory optimization framework, we conducted a series of comparative experiments focusing on two core aspects: (i) the learning performance measured by cumulative reward, and (ii) the task execution efficiency reflected by episode length. This section presents a quasi-ablation study comprising seven variants of the PPO-based model, where the baseline PPO is compared with models incorporating residual blocks and various temporal modeling modules, including LSTM, Bi-LSTM, GRU, Bi-GRU, RNN, and Bi-RNN. Each model is assessed across multiple metrics to reveal its respective advantages and limitations.

4.2.1. Reward-Based Analysis: Policy Learning Efficiency and Robustness

Cumulative reward serves as a primary indicator of the policy's quality and learning progress. As illustrated in Figure 7, the Lstm-ResB-PPO model converges substantially faster, achieving a stable reward level within 520,000 steps. In contrast, the baseline PPO requires 1,000,000 steps to attain comparable performance. The Lstm-ResB-PPO model achieves a higher final reward of 861.138, exceeding the 852.301 achieved by the baseline PPO. It also reaches a peak reward of 877.502, which surpasses the baseline's maximum of 869.986, thereby demonstrating improved learning efficiency and enhanced exploratory capability.

In terms of stability, the enhanced model exhibits minimal fluctuation, with only a single observed drop in reward during training. By contrast, other variants based on GRU and Bi-GRU architectures display pronounced instability, characterized by five and seven major reward oscillations, respectively. Models incorporating RNN-type modules generally fail to converge to meaningful reward values; for instance, the Bi-RNN variant reaches a final reward as low as -4695.173. In other cases, such models remain confined to low-reward regions throughout training. These results collectively support the advantage of combining residual structure with LSTM in balancing expressiveness and stability. Table 6 summarizes the key metrics data for both algorithms during the training process, which reports, for all model variants, the Convergence Step (CS), Final Performance (FP), Converged Performance (CP), Peak Reward (PR), Minimum Reward (MR), and the Number of Fluctuations (NF).

4.2.2. Episode Length Analysis: Task Completion Efficiency

Complementing the reward-based analysis, we evaluate the average episode length, which reflects how efficiently the agent can complete tasks. In Figure 8, the LSTM-ResB-PPO achieves rapid convergence to a stable episode length of 147 within 520,000 steps, while the final value is comparable to that of the baseline PPO, the training speed of the LSTM-ResB-PPO is significantly faster. This suggests that the residual-enhanced LSTM structure not only improves reward acquisition but also accelerates the learning of efficient task execution. Alternative temporal encoders demonstrate mixed performance outcomes. For example, the RNN-based variants, including both unidirectional and bidirectional implementations, achieve relatively shorter episode lengths of 115 and 114.688, respectively. However, this reduction in episode length is accompanied by unstable reward trajectories and a greater number of fluctuations, which compromise overall training stability. Notably, Bi-GRU exhibits a shorter episode length but suffers from poor reward performance and high volatility. This discrepancy indicates that shorter episodes do not necessarily correlate with better policy quality in the absence of stable learning dynamics. A comparative summary of key performance metrics is presented in Table 7, which reports,

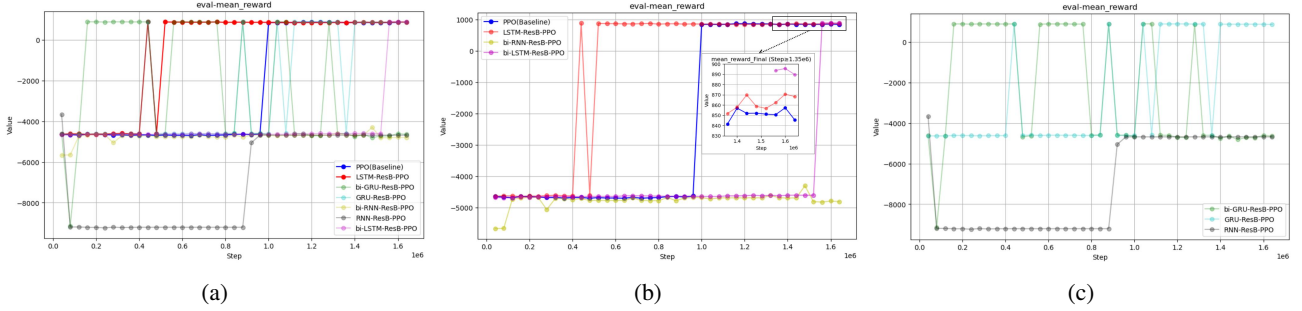


Figure 7. Line Graph Comparing the Change of Mean Reward with the Number of Training Steps for Different Algorithm Training Processes, Where (a) Shows the Training Performance of All Algorithms, (b) Shows the Performance of Algorithms that Converged after Training, and (c) Shows the Performance of Algorithms that did not Converge after Training.

Table 6

Performance Comparison of Different Algorithms about Mean Reward.

Algorithm	CS	FP	CP	PR	MR	NF
PPO Baseline[19]	1000000	822.301	855.022	869.986	841.548	0
lstm-ResB PPO	520000	861.138	861.055	877.502	851.776	1
bi-lstm-ResB PPO	1560000	-2541.737	893.035	895.653	889.659	0
rnn-ResB PPO	960000	-4683.867	-4683.656	-4680.461	-4683.867	0
bi-rnn-ResB PPO	1520000	-4695.173	-4802.599	-4782.936	-4815.568	2
gru-ResB PPO	-	185.280	-	-	-	5
bi-gru-ResB PPO	-	-4687.911	-	-	-	7

for all model variants, the CS, FP, CP, Peak Episode Length (PEL), Minimum Episode Length (MEL), and NF.

4.2.3. Summary and Cross-Metric Synthesis

A comparative analysis of key performance metrics is provided in Table 6 and 7, covering reward trends and episode lengths across all model variants. The Lstm-ResB-PPO model demonstrates the most consistent and effective performance, converging 48 percent faster than the baseline with significantly improved reward acquisition and execution stability. It achieves higher peak and final rewards, maintains efficient episode lengths, and exhibits minimal fluctuations, indicating strong robustness during training. In contrast, alternative temporal encoders either fail to stabilize or sacrifice reward quality in pursuit of shorter episodes. These results underscore the critical role of structural synergy in temporal modeling and confirm that the residual-enhanced LSTM architecture is particularly well-suited for

the demands of assistive trajectory optimization, where stable policy learning and reliable execution are essential to ensuring safe and effective navigation support for visually impaired users.

4.3. Safety-Oriented Evaluation of Cost and Risk Metrics

To comprehensively assess the impact of momentum-informed optimization and residual-enhanced temporal modeling on strategy safety and cost efficiency, this section presents a comparative evaluation between the baseline PPO and the proposed LSTM-ResB-PPO model. The analysis focuses on four key indicators: average cost, cost variance, ego risk, and obstacle risk. All metrics are computed over the training window associated with the final deployed policy for each algorithm.

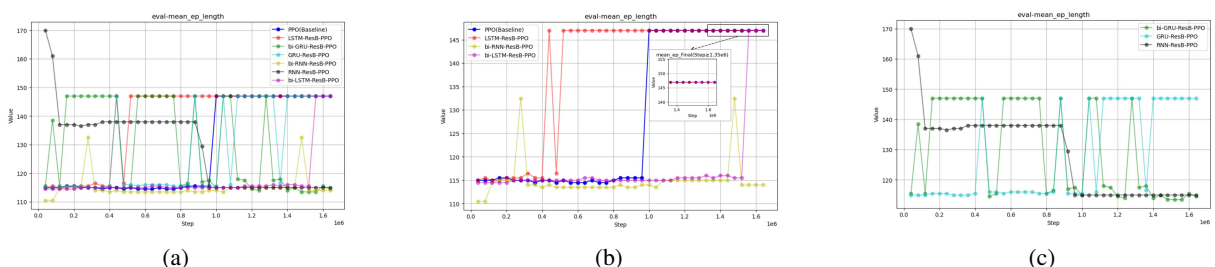


Figure 8. Line Graph Comparing the Change of Average Ep Length with the Number of Training Steps for Different Algorithm Training Processes, where (a) Shows the Training Performance of All Algorithms, (b) Shows the Performance of Algorithms that Converged after Training, and (c) Shows the Performance of Algorithms that did not Converge after Training.

Table 7

Performance Comparison of Different Algorithms about Mean Ep Length.

Algorithm	CP	FP	CP	PEL	MEL	NF
PPO Baseline[19]	1000000	147	147	147	147	0
Istm-ResB PPO	520000	147	147	147	147	1
bi-Istm-ResB PPO	1560000	127.438	147	147	147	0
rnn-ResB PPO	960000	115	115	115	115	0
bi-rnn-ResB PPO	1520000	116.688	114	114	114	2
gru-ResB PPO	-	143.188	-	-	-	5
bi-gru-ResB PPO	-	114.688	-	-	-	7

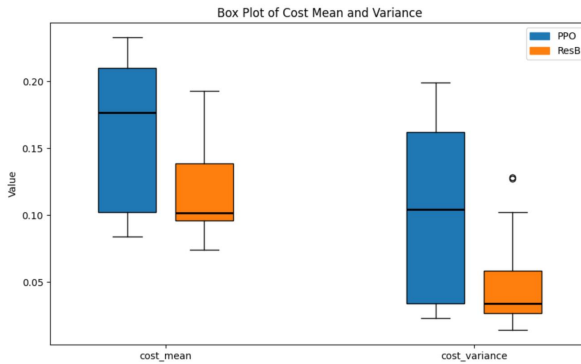


Figure 9. Box Plots of Cost Metrics for the Two Algorithms Best Model, including Mean and Variance of Cost.

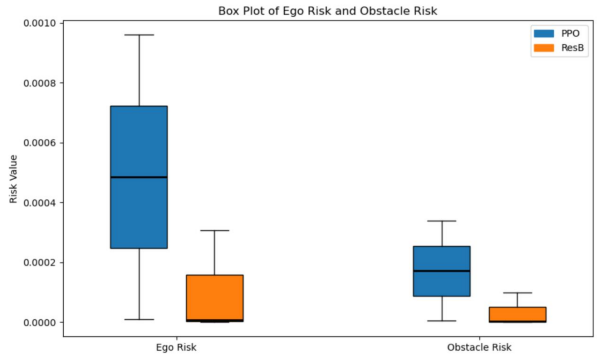


Figure 10. Box Plots of Risk Metrics for the Two Algorithms Best Model, including Mean and Variance of Cost.

4.3.1. Cost Reduction and Planning Robustness

The first set of results, visualized through cost-related boxplots, examines the mean and variance of the cumulative cost incurred during training. As illustrated in Figure 9, the LSTM-ResB-PPO model achieves a marked reduction in both metrics. The average cost mean is reduced from 0.166472 in the baseline PPO to 0.116065, reflecting a relative decrease of approximately 30.3%. Simultaneously, the cost variance is lowered from 0.102921 to 0.048067, denoting a 53.3% improvement in planning consistency. These reductions indicate that the enhanced architecture not only guides the agent toward more cost-efficient decision paths but also mitigates volatility in cost outcomes across episodes, thereby contributing to improved robustness during deployment.

4.3.2. Risk Minimization and Policy Safety

In addition to cost control, the evaluation includes a safety analysis focusing on risk[50] exposure. Two domain-specific risk metrics are employed in the evaluation. Ego risk quantifies the agent's exposure to self-induced hazards arising from suboptimal motion states, such as excessive velocity or unsafe turning behavior. Obstacle risk reflects the degree of potential collision or proximity danger in relation to surrounding environmental objects. Comparing ego risk and obstacle risk, Figure 10 is shown below.

Boxplot analysis and aggregated data in Table 8 demonstrate a significant performance margin in favor of the LSTM-ResB-PPO model. The average ego risk is reduced from 4.85×10^{-4} to 1.05×10^{-4} , representing a 77.2%

reduction. Meanwhile, the obstacle risk drops from 1.72×10^{-4} to 3.34×10^{-5} , highlighting the model's enhanced ability to navigate safely within dynamic environments.

4.3.3. Integrated Analysis and Scenario Relevance

When considering both cost and risk evaluations, the LSTM-ResB-PPO model consistently demonstrates superior performance. It generates more stable and economical trajectory plans while exhibiting greater resilience to environmental uncertainty and physical constraints. These improvements are particularly beneficial in assistive navigation scenarios for the visually impaired, where both efficiency and safety are critical. The observed advantages stem from the synergy of two key enhancements: the residual-enhanced LSTM architecture, which strengthens temporal feature modeling and learning stability; and the momentum-informed trajectory optimization, which incorporates virtual force constraints to guide safer and more adaptive planning. Together, these components yield a well-balanced strategy that effectively reduces cost, suppresses risk, and enhances policy robustness in dynamic environments.

4.4. Simulation-Based Evaluation and Quantitative Assessment

Building upon the scenario selection strategy detailed in the training setup, this section presents a comprehensive evaluation of the proposed LSTM-ResB-PPO framework through both visualized simulations and quantitative performance metrics. The goal is to assess the model's ability to meet the planning demands of assistive navigation under

Table 8

Cost and Risk Metrics for Best Models

Algorithm	Cost		Risk	
	Avg. Cost-mean	Avg. Cost-variance	Avg. Risk-ego.	Avg. Risk-obs.
PPO (Baseline)[19]	0.166472	0.102921	4.848913×10^{-4}	1.716621×10^{-4}
LSTM-ResB-PPO	0.116065	0.048067	1.053492×10^{-4}	3.336874×10^{-5}

Table 9

Simulation Scenario Properties

Scenarios validation test	DEL_Lengde-21_1_T-15	USA_Lanker-1_7_T-1	ZAM_Junction-1_1_19_T-1
Data Source	Scenario Factory 2.0 - SUMO	Generation (NGSIM), OSM	Specification-based scenario synthesis
Obstacle Behavior Type	TRAJECTORY	TRAJECTORY	TRAJECTORY
Scenario Tags	INTERSECTION, MERGING LANES, SIMULATED, SINGLE LANE	ONCOMING TRAFFIC, COMFORT, URBAN, INTERSECTION, LANE FOLLOWING	ONCOMING TRAFFIC, TURN LEFT, URBAN, INTERSECTION
Obstacle Classes	CAR	CAR	CAR
Goal Types	POSITION, TIME_STEP	ORIENTATION, VELOCITY, TIME_STEP	LANEFT, VELOCITY, TIME_STEP
Scenario Duration	15.10 s	1.50 s	14.70 s
Initial Velocity	5.11 m/s	9.73 m/s	5.16 m/s
No. of Static Obstacles	0	0	0
No. of Dynamic Obstacles	89	22	5
No. of Ego Vehicles	1	1	1

realistic and dynamic scenarios. To ensure robustness and generalizability, three representative CommonRoad scenarios are selected, each characterized by dynamic obstacle behaviors, road semantic features such as intersections and merging lanes, and moderate complexity in obstacle density and velocity. The simulation attributes, including obstacle types, goal definitions, initial speeds, and obstacle counts, are summarized in Table 9 to ensure experimental transparency and reproducibility.

4.4.1. Visualized Behavior Analysis

To analyze the planning quality and behavioral dynamics, two scenarios are selected for visual illustration. For each, a series of trajectory-level indicators are plotted: (i) the executed global path, (ii) temporal profiles of velocity and acceleration, (iii) cumulative weighted planning cost over time, and (iv) cumulative change in action prediction, which reflects the decision trend of the policy network and serves as a proxy for behavioral consistency.

In the DEU_Lengede-21_1_T-15 scenario shown in Figure 11, a distinct contrast emerges between the proposed LSTM-ResB-PPO framework and the baseline PPO in terms of task completion, behavioral safety, and dynamic consistency. As illustrated in the trajectory visualization, the baseline model fails to complete the navigation task and exhibits hazardous behavior by deviating into the oncoming traffic lane. This erroneous planning outcome not only violates traffic semantics but also poses significant collision risks.

In contrast, the LSTM-ResB-PPO model successfully navigates along the correct lane throughout the entire planning horizon, demonstrating an effective understanding of lane topology and interaction constraints.

The velocity and acceleration profiles further reveal the advantages of the proposed framework in ensuring planning smoothness and passenger comfort. In the later stages of the trajectory, the LSTM-ResB-PPO model exhibits a gradual and controlled reduction in velocity. The velocity-time curve maintains a smooth gradient, indicating that deceleration is achieved without abrupt maneuvers. This behavior aligns with safety-sensitive planning principles in assistive navigation, where sudden changes may disorient or endanger visually impaired users. Correspondingly, the acceleration profile remains within moderate bounds, with no discontinuities, validating the model's capability for stable motion execution. The variation of velocity and acceleration with respect to the s-direction in this scenario is depicted in Figure 12.

Moreover, analysis of the cumulative weighted cost confirms the optimization efficiency of the proposed approach. Throughout the planning process, the cumulative cost of LSTM-ResB-PPO remains consistently lower than that of the baseline, implying more efficient trajectory selection with reduced trade-off between distance, time, and risk. The cumulative predicted action deviation metric further

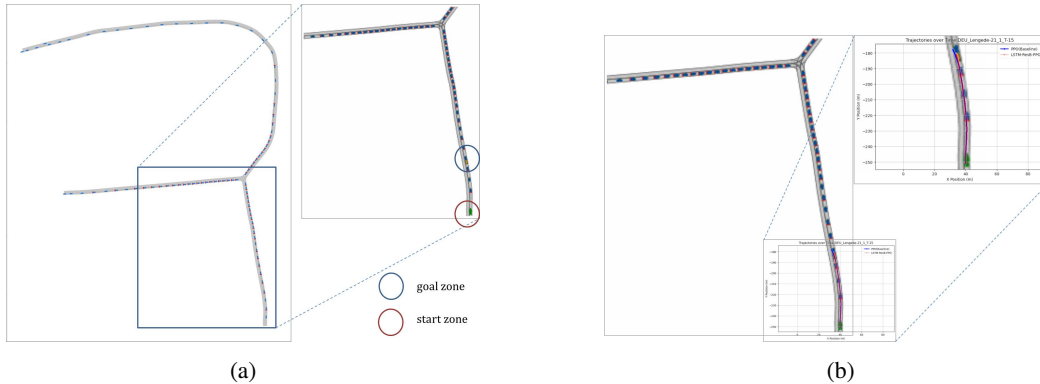


Figure 11. Visualization of the DEU_Lengede-21_1_T-15 Scenario, where (a) Highlights the Marked Planning Start and Goal Zones, and (b) Illustrates the Trajectory Planning Results of Two Algorithms.

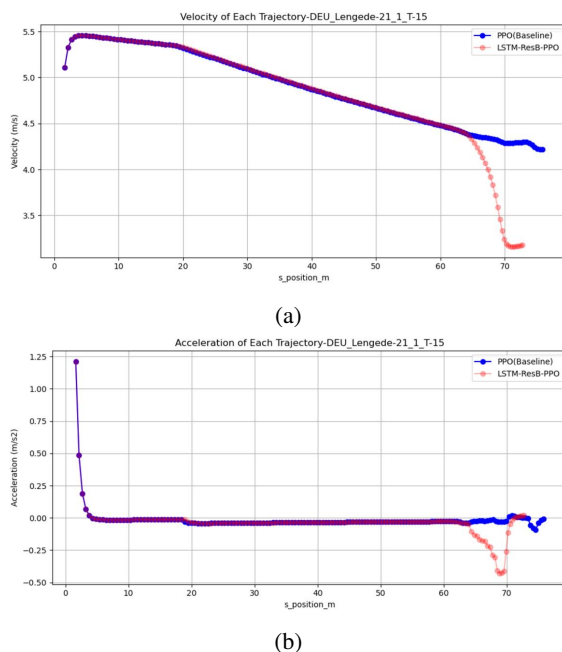


Figure 12. Speed and Acceleration Curves along the S-direction Position for Two Algorithms under the DEU_Lengede-21_1_T-15 Scenario: (a) Speed Curves; (b) Acceleration Curves.

distinguishes the two models. The baseline exhibits a progressively increasing trend. In contrast, the LSTM-ResB-PPO model demonstrates a convergent downward trend, reflecting both temporal consistency and policy reliability. In this scenario, the evolution of the cumulative weighted cost and the cumulative predicted action along the s-direction is illustrated in the subsequent Figure 13.

Overall, this case study highlights the superiority of the LSTM-ResB-PPO framework in generating safe, efficient, and behaviorally consistent plans in a high-risk intersection. The model not only avoids failure cases typical of conventional policies but also adheres to assistive navigation requirements such as directional correctness, dynamic stability, and long-horizon decision robustness.

The ZAM_Tjunction-1_119_T-1 scenario shown in Figure 14 presents a goal condition requiring the agent to reach a specified velocity and positional region. Both the baseline PPO and the proposed LSTM-ResB-PPO successfully satisfy these criteria; however, their performance diverges notably in terms of trajectory smoothness, dynamic behavior, and cost control.

Figure 15 shows that while the overall path shapes of both models appear similar, the LSTM-ResB-PPO agent traverses a marginally longer distance. This deviation, upon closer examination of the velocity and acceleration profiles, is revealed to be the result of more refined motion segmentation and smoother control transitions. The trajectory can be interpreted in three distinct phases: (1) a left-turn maneuver, (2) a deceleration segment aimed at reaching the goal velocity, and (3) a final stabilization phase before goal attainment. In this scenario, the changes in velocity and acceleration as functions of the s-direction are presented in the accompanying figure. During the initial left-turn phase, the agent must yield to an oncoming vehicle, introducing a safety-critical constraint. In this segment, the LSTM-ResB-PPO model exhibits a significantly more stable velocity profile, in contrast to the baseline PPO, which shows pronounced peaks in both velocity and acceleration. The absence of such spikes in the proposed model indicates a superior capacity to handle dynamic interactions without inducing abrupt motions, thereby enhancing both safety and comfort. In the subsequent deceleration phase, where the agent begins reducing speed to meet the goal velocity, the proposed framework again demonstrates smoother control. Notably, despite the absence of static or dynamic obstacles in this region, the LSTM-ResB-PPO model executes a gradual and continuous deceleration, avoiding aggressive braking and maintaining a consistent velocity gradient.

Finally, in the stabilization phase, the model enters a slow-speed regime and converges gently towards the predefined target velocity. The smoother decline in the velocity curve for LSTM-ResB-PPO illustrates the model's capacity to finely regulate low-speed behavior, a critical aspect in assistive navigation where abrupt halts or oscillations can compromise user safety and trust.

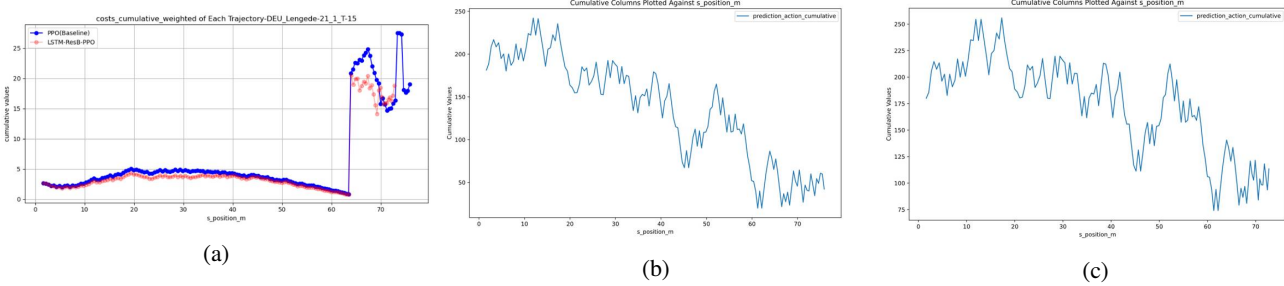


Figure 13. Variation of Cumulative Weighted Cost and Cumulative Predicted Action with S-direction Position for Two Algorithms under the DEU_Lengede-21_1_T-15 Scenario: (a) Line Comparison of Cumulative Weighted Cost for Both Algorithms; (b) Line Variation of Cumulative Predicted Action for LSTM-ResB-PPO; (c) Line Variation of Cumulative Predicted Action for the Baseline Algorithm.

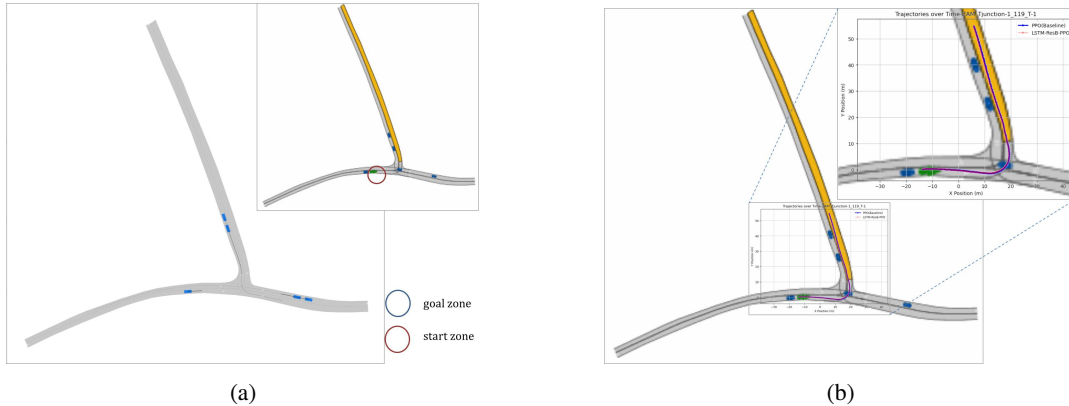


Figure 14. Visualization of the ZAM_Tjunction-1_119_T-1 Scenario, where (a) Highlights the Marked Planning Start and Goal Zones, and (b) Illustrates the Trajectory Planning Results of Two Algorithms.

In this scenario, the cumulative weighted cost and the cumulative predicted action are shown to vary with the s-direction in following Figure 16. Regarding cost-related metrics, the cumulative weighted cost for LSTM-ResB-PPO remains consistently lower, with significantly fewer abrupt spikes than the baseline. This reduction reflects the model's efficiency in optimizing multi-objective cost terms throughout the planning horizon. Additionally, in the cumulative predicted action deviation metric, both models exhibit a downward trend, indicating risk-aware trajectory predictions. However, the smoother and more monotonic decline observed in the proposed model further confirms its enhanced temporal consistency and lower planning uncertainty.

In summary, this case study reinforces the advantages of the LSTM-ResB-PPO framework in achieving not only goal-directed success but also higher-order qualities such as smoothness, stability, and cost-efficient planning. Its behavior aligns well with the nuanced requirements of visually impaired navigation scenarios, where maintaining low-risk, human-friendly motion is essential. In both scenarios, the LSTM-ResB-PPO model not only accomplishes the planning objectives but also generates smoother and more continuous trajectories with stable speed and acceleration profiles, indicating improved execution comfort and physical feasibility. The cumulative cost exhibits a consistently

moderate and convergent trend, reflecting effective path optimization. Furthermore, the prediction consistency curves display lower volatility and steady decline, underscoring the model's temporal stability, risk awareness, and robustness in high-level decision-making.

4.4.2. Quantitative Metric Evaluation

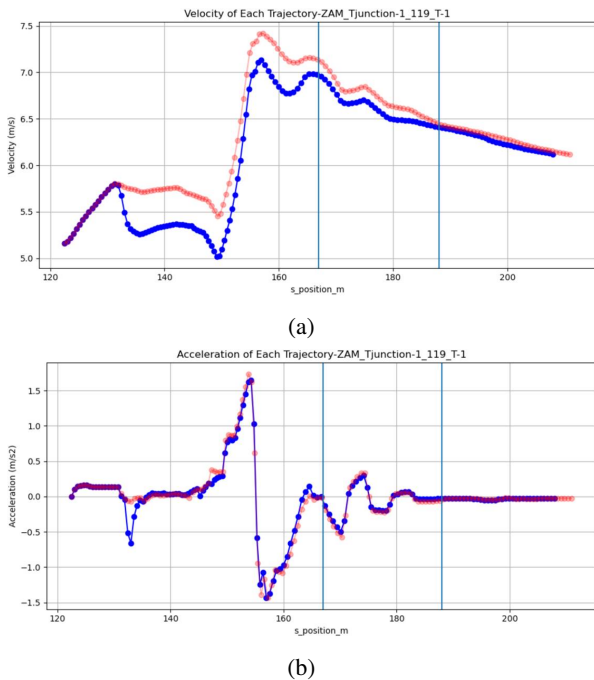
To further substantiate the advantages of the proposed framework, Table 10 compares the LSTM-ResB-PPO and baseline PPO algorithms across three selected scenarios using four metrics: goal achievement rate, number of generated trajectory clusters, average self-risk, and cumulative weighted cost. These metrics collectively evaluate planning feasibility, computational efficiency, safety performance, and optimization quality.

The LSTM-ResB-PPO consistently achieves full task completion across all scenarios, outperforming the baseline in both safety and cost indicators. Specifically, the model yields shorter or equivalent trajectory cluster counts, indicating improved planning efficiency without sacrificing diversity. Average ego risk is significantly reduced, evidencing the model's ability to mitigate self-induced motion hazards. Furthermore, cumulative costs are consistently lower, reflecting the impact of temporal modeling and residual enhancement on long-term decision optimization.

Table 10

Performance Comparison of Algorithms Across Different Scenarios

Scenarios	Algorithm	Goal reached	Number of trajectory clusters	Avg. Ego-risk	Avg. Costs
DEU_Lengede-21_1_T-15	PPO (Baseline)[19]	0	152	2.25395e-14	6.6384
	LSTM-ResB-PPO	1	150	8.4692e-16	5.4286
ZAM_Junction-1_119_T-1	PPO (Baseline)[19]	1	146	9.7826e-05	53.015
	LSTM-ResB-PPO	1	146	8.9332e-05	36.3689
USA_Tanker-1_7_T-1	PPO (Baseline)[19]	1	13	3.2864e-05	31.5190
	LSTM-ResB-PPO	1	13	3.2864e-05	30.6837

**Figure 15.** Speed and Acceleration Curves Along the S-direction Position for Two Algorithms under the ZAM_Tjunction-1_119_T-1 Scenario: (a) Speed Curves; (b) Acceleration Curves.

4.4.3. Discussion

These findings collectively validate the efficacy of the proposed trajectory optimization framework in assistive navigation contexts. The integration of LSTM-based temporal modeling and residual blocks not only improves policy stability and behavioral smoothness but also enables a favorable trade-off between exploration efficiency and conservative decision-making. Coupled with momentum-aware trajectory optimization constraints implicitly embedded in the DRL structure, the model exhibits strong adaptability across diverse scenes involving uncertainty, interaction, and physical limitations.

Overall, the simulation-based analysis confirms that LSTM-ResB-PPO offers a reliable and scalable solution for safety-critical, comfort-sensitive planning tasks, establishing a solid foundation for downstream deployment in real-world assistive trajectory optimization framework.

5. Conclusion

This paper proposed a human-centered MHHTOF framework that integrated HTSCMOE with a residual-enhanced DRL policy, enabling semantically aligned and dynamically feasible trajectory planning for assistive navigation. By employing a unified multi-objective cost formulation and a weight transfer mechanism across Frenet and Cartesian stages, the method ensured consistent optimization while enhancing personalization for visually impaired users. The incorporation of LSTM-based temporal modeling and residual connections improved policy stability and expressiveness. Extensive simulations validated the superiority of the proposed LSTM-ResB-PPO over PPO baselines, demonstrating faster convergence, higher peak reward, reduced variance, and significant reductions in both cost and risk metrics, thereby affirming its effectiveness in safety-critical and comfort-sensitive planning tasks.

References

- [1] A. P. Kalidas, C. J. Joshua, A. Q. Md, S. Basheer, S. Mohan, S. Sakri, Deep reinforcement learning for vision-based navigation of uavs in avoiding stationary and mobile obstacles, *Drones* 7 (4) (2023) 245.
- [2] A. B. Najjar, A. R. Al-Issa, M. Hosny, Dynamic indoor path planning for the visually impaired, *Journal of King Saud University-Computer and Information Sciences* 34 (9) (2022) 7014–7024.
- [3] S. M. Shin, J. Lim, Y. Choi, Guide dog ar: A tactile and auditory assisting device design with the motif of a guide dog for the visually impaired, *International Journal of Human-Computer Interaction* (2024) 1–14.
- [4] H. R. Surougi, J. A. McCann, Real-time optimisation-based path planning for visually impaired people in dynamic environments, in: *Proceedings of the IEEE/CVF International Conference on Computer Vision*, 2023, pp. 1839–1848.
- [5] I. Patel, M. Kulkarni, N. Mehendale, Review of sensor-driven assistive device technologies for enhancing navigation for the visually impaired, *Multimedia Tools and Applications* 83 (17) (2024) 52171–52195.
- [6] S. Teng, X. Hu, P. Deng, B. Li, Y. Li, Y. Ai, D. Yang, L. Li, Z. Xuanyuan, F. Zhu, et al., Motion planning for autonomous driving: The state of the art and future perspectives, *IEEE Transactions on Intelligent Vehicles* 8 (6) (2023) 3692–3711.
- [7] N. Fernando, D. A. McMeekin, I. Murray, Route planning methods in indoor navigation tools for vision impaired persons: a systematic review, *Disability and Rehabilitation: Assistive Technology* 18 (6) (2023) 763–782.
- [8] W. Nawaz, K. U. Khan, K. Bashir, A review on path selection and navigation approaches towards an assisted mobility of visually impaired people, *KSII Transactions on Internet and Information Systems (TIIS)* 14 (8) (2020) 3270–3294.

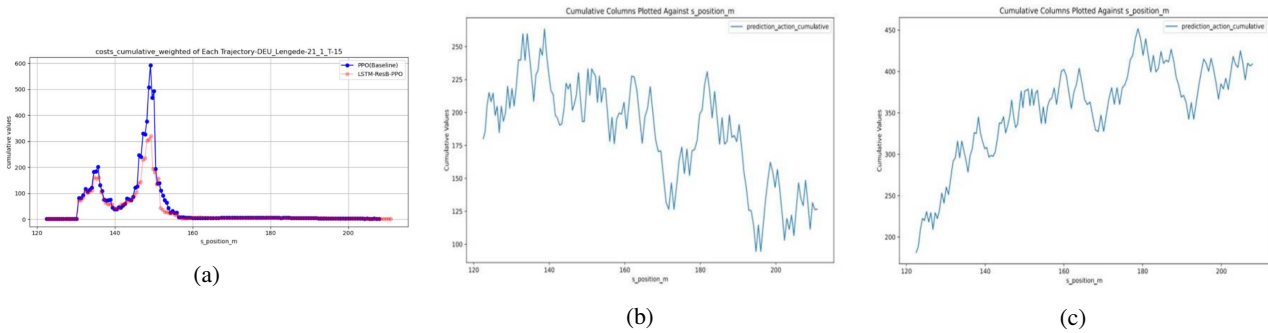


Figure 16. Variation of Cumulative Weighted Cost and Cumulative Predicted Action with S-direction Position for Two Algorithms under the ZAM_Tjunction-1_119_T-1 Scenario: (a) Line comparison of Cumulative Weighted Cost for Both Algorithms; (b) Line Variation of Cumulative Predicted Action for LSTM-ResB-PPO; (c) Line Variation of Cumulative Predicted Action for the Baseline Algorithm.

[9] D. Chen, S. Li, J. Wang, Y. Feng, Y. Liu, A multi-objective trajectory planning method based on the improved immune clonal selection algorithm, *Robotics and computer-integrated manufacturing* 59 (2019) 431–442.

[10] P. Balatti, I. Ozdamar, D. Sirintuna, L. Fortini, M. Leonori, J. M. Gandarias, A. Ajoudani, Robot-assisted navigation for visually impaired through adaptive impedance and path planning, in: 2024 IEEE International Conference on Robotics and Automation (ICRA), IEEE, 2024, pp. 2310–2316.

[11] C. Zhang, W. Xu, Intelligent vehicle path based on discretized sampling points and improved cost function: A quadratic programming approach, *IEEE Access* 12 (2024) 24500–24515.

[12] J. Wang, L. Chu, Y. Zhang, Y. Mao, C. Guo, Intelligent vehicle decision-making and trajectory planning method based on deep reinforcement learning in the frenet space, *Sensors* 23 (24) (2023) 9819.

[13] S. Siboo, A. Bhattacharyya, R. Naveen Raj, S. H. Ashwin, An empirical study of ddpg and ppo-based reinforcement learning algorithms for autonomous driving, *IEEE Access* 11 (2023) 125094–125108. doi:10.1109/ACCESS.2023.3330665.

[14] Q. Xiao, L. Jiang, M. Wang, X. Zhang, An improved distributed sampling ppo algorithm based on beta policy for continuous global path planning scheme, *Sensors* 23 (13) (2023) 6101.

[15] R. Zhang, J. Hou, G. Chen, Z. Li, J. Chen, A. Knoll, Residual policy learning facilitates efficient model-free autonomous racing, *IEEE Robotics and Automation Letters* 7 (4) (2022) 11625–11632.

[16] S. Wen, Y. Shu, A. Rad, Z. Wen, Z. Guo, S. Gong, A deep residual reinforcement learning algorithm based on soft actor-critic for autonomous navigation, *Expert Systems with Applications* 259 (2025) 125238.

[17] R. Zhang, X. Qin, M. Pan, S. Li, H. Shen, Adaptive temporal reinforcement learning for mapping complex maritime environmental state spaces in autonomous ship navigation, *Journal of Marine Science and Engineering* 13 (3) (2025) 514.

[18] Z. Zhang, C. Shi, P. Zhu, Z. Zeng, H. Zhang, Autonomous exploration of mobile robots via deep reinforcement learning based on spatiotemporal information on graph, *Applied Sciences* 11 (18) (2021) 8299.

[19] R. Trauth, A. Hobmeier, J. Betz, A reinforcement learning-boosted motion planning framework: Comprehensive generalization performance in autonomous driving, in: 2024 IEEE Intelligent Vehicles Symposium (IV), IEEE, 2024, pp. 2413–2420.

[20] S. Zhao, S.-H. Hwang, Exploration-and exploitation-driven deep deterministic policy gradient for active slam in unknown indoor environments, *Electronics* 13 (5) (2024) 99.

[21] B. Li, Y. Ouyang, L. Li, Y. Zhang, Autonomous driving on curvy roads without reliance on frenet frame: A cartesian-based trajectory planning method, *IEEE Transactions on Intelligent Transportation Systems* 23 (9) (2022) 15729–15741.

[22] M. Morsali, E. Frisk, J. Åslund, Spatio-temporal planning in multi-vehicle scenarios for autonomous vehicle using support vector machines, *IEEE Transactions on Intelligent Vehicles* 6 (4) (2020) 611–621.

[23] B. Li, Y. Zhang, Fast trajectory planning in cartesian rather than frenet frame: A precise solution for autonomous driving in complex urban scenarios, *IFAC-PapersOnLine* 53 (2) (2020) 17065–17070.

[24] M. Morsali, E. Frisk, J. Åslund, Spatio-temporal planning in multi-vehicle scenarios for autonomous vehicle using support vector machines, *IEEE Transactions on Intelligent Vehicles* 6 (4) (2020) 611–621.

[25] Y. Zhang, S. Wang, Lspp: A novel path planning algorithm based on perceiving line segment feature, *IEEE Sensors Journal* 22 (1) (2021) 720–731.

[26] K. Shu, N.-D. Đào, W. Shi, A. Khajepour, Group frenet frame cav path planning on highways, *IEEE Internet of Things Journal* 11 (4) (2023) 6776–6787.

[27] J. Huang, Z. He, Y. Arakawa, B. Dawton, Trajectory planning in frenet frame via multi-objective optimization, *IEEE Access* 11 (2023) 70764–70777.

[28] Y. Wang, Z. Lin, Research on path planning for autonomous vehicle based on frenet system, *Journal of engineering research* 11 (2) (2023) 100080.

[29] J. Wang, J. Wu, X. Zheng, D. Ni, K. Li, Driving safety field theory modeling and its application in pre-collision warning system, *Transportation research part C: emerging technologies* 72 (2016) 306–324.

[30] R. Zhang, H. Guo, M. A. Sotelo, H. Du, A. Darius, Z. Li, New rrt-based method for vehicle path planning in curve scenarios considering path oscillations, *IEEE Transactions on Vehicular Technology* (2025).

[31] A. Bajpai, A. Lu, K. Choi, R. Tayal, A. Young, A. Mazumdar, Improving human situational awareness and planning using a human-centric velocity-obstacle algorithm, *ACM Transactions on Human-Robot Interaction* 14 (3) (2025) 1–28.

[32] B. Zhao, Y. Wu, C. Wu, R. Sun, Deep reinforcement learning trajectory planning for robotic manipulator based on simulation-efficient training, *Scientific Reports* 15 (1) (2025) 8286.

[33] Y. Qin, Y. Huang, W. Yu, H. Wang, Roitp: Road obstacle-involved trajectory planner for autonomous trucks, *Chinese Journal of Mechanical Engineering* 38 (1) (2025) 9.

[34] M. Jin, M. Qu, Q. Gao, Z. Huang, T. Su, Z. Liang, Advanced trajectory planning and control for autonomous vehicles with quintic polynomials, *Sensors* 24 (24) (2024) 7928.

[35] X. Qian, F. Alché, P. Bender, C. Stiller, A. de La Fortelle, Optimal trajectory planning for autonomous driving integrating logical constraints: An miqp perspective, in: 2016 IEEE 19th international conference on intelligent transportation systems (ITSC), IEEE, 2016, pp. 205–210.

[36] J. Wang, J. Wu, Y. Li, The driving safety field based on driver–vehicle–road interactions, *IEEE Transactions on Intelligent Transportation Systems* 16 (4) (2015) 2203–2214.

- [37] D. Helbing, J. Keltsch, P. Molnar, Modelling the evolution of human trail systems, *Nature* 388 (6637) (1997) 47–50.
- [38] K. Chu, M. Lee, M. Sunwoo, Local path planning for off-road autonomous driving with avoidance of static obstacles, *IEEE transactions on intelligent transportation systems* 13 (4) (2012) 1599–1616.
- [39] C. Zhang, D. Chu, S. Liu, Z. Deng, C. Wu, X. Su, Trajectory planning and tracking for autonomous vehicle based on state lattice and model predictive control, *IEEE Intelligent Transportation systems magazine* 11 (2) (2019) 29–40.
- [40] R. Trauth, K. Moller, G. Würsching, J. Betz, Frenetix: A high-performance and modular motion planning framework for autonomous driving, *IEEE Access* (2024).
- [41] B. Brito, A. Agarwal, J. Alonso-Mora, Learning interaction-aware guidance policies for motion planning in dense traffic scenarios, *arXiv preprint arXiv:2107.04538* (2021).
- [42] J. Schulman, F. Wolski, P. Dhariwal, A. Radford, O. Klimov, Proximal policy optimization algorithms, *arXiv preprint arXiv:1707.06347* (2017).
- [43] S. Hochreiter, J. Schmidhuber, Long short-term memory, *Neural computation* 9 (8) (1997) 1735–1780.
- [44] K. He, X. Zhang, S. Ren, J. Sun, Deep residual learning for image recognition, in: *Proceedings of the IEEE conference on computer vision and pattern recognition*, 2016, pp. 770–778.
- [45] D. Dakopoulos, N. G. Bourbakis, Wearable obstacle avoidance electronic travel aids for blind: a survey, *IEEE Transactions on Systems, Man, and Cybernetics, Part C (Applications and Reviews)* 40 (1) (2009) 25–35.
- [46] A. Fertig, L. Balasubramanian, M. Botsch, Hybrid machine learning model with a constrained action space for trajectory prediction, *arXiv preprint arXiv:2501.03666* (2025).
- [47] H. Khan, T. D. Chaudhari, J. V. N. Ramesh, A. S. Kranthi, E. Muniyandy, Y. A. B. El-Ebary, D. N. P. Devadhas, Neuro-symbolic reinforcement learning for context-aware decision making in safe autonomous vehicles., *International Journal of Advanced Computer Science & Applications* 16 (5) (2025).
- [48] C. Glanois, P. Weng, M. Zimmer, D. Li, T. Yang, J. Hao, W. Liu, A survey on interpretable reinforcement learning, *Machine Learning* 113 (8) (2024) 5847–5890.
- [49] M. Althoff, M. Koschi, S. Manzinger, Commonroad: Composable benchmarks for motion planning on roads, in: *2017 IEEE Intelligent Vehicles Symposium (IV)*, IEEE, 2017, pp. 719–726.
- [50] M. Geisslinger, F. Poszler, M. Lienkamp, An ethical trajectory planning algorithm for autonomous vehicles, *Nature Machine Intelligence* 5 (2) (2023) 137–144.